ROYAL SOCIETY OF CHEMISTRY

PAPER

Check for updates

Mitigating effect of organic matter on the *in vivo* toxicity of metal oxide nanoparticles in the marine environment†

Seta Noventa, [iD] * Darren Rowe and Tamara Galloway

Major constituents of seawater, *i.e.* ions and natural organic matter (NOM), can influence the environmental and toxicological behaviour of nanoparticles (NPs) in aquatic systems. By adsorbing–ligating–reacting to NP surface reactive sites, they can modify the NP surface structure and overall physico-chemical proprieties. This study explored the fate and *in vivo* toxicity of ZnO and MnO_2 NPs under artificial seawater conditions. These two nanomaterials are representative of metal oxide NPs inducing harm *via* dissolution and bandgap mechanisms, respectively. To gain a comprehensive understanding of the overall toxicological outcome, we traced the behaviour of NPs in the test systems (*i.e.* aggregation, sedimentation, dissolution, sorption), their fate in the model organism (*i.e.* ingestion and cellular internalization by oyster larvae), and the induction of a toxicological pathway (*i.e.* oxidative stress) up to pathogenesis. We found that ZnO NPs induced harm to oyster larvae under seawater conditions, but NOM mitigated its intensity. In contrast, MnO_2 NPs were not toxic at the tested concentrations (up to 200 μM), and their toxicological stasis was not modified by the presence of organic matter. We propose that strong ion sorption on the MnO_2 NP surface blocked redox-active sites thus preventing their bandgap mode of action.

Environmental significance

Understanding how environmentally-driven transformations alter the toxicity of manufactured nanomaterials is fundamental for the development of safe nanotechnologies. Structure–activity paradigms that are central to predicting the toxicity of nanomaterials in *in vitro* systems might be ineffective when applied to real environmental scenarios. By focusing on two model metal oxide nanoparticles (NPs), this study provides a comprehensive picture of the efficiency of two promising paradigms (*i.e.* dissolution and bandgap) to predict NP toxicity under marine-like conditions. Furthermore, it highlights that other NPs proprieties, such as the sorption capacity, can be of primary importance to consider in marine studies.

1 Introduction

There are many ways in which metal oxide nanoparticles (NPs) can cause toxicity. These relate to both the toxicity of the metal ions from which they are composed and to the physico-chemical characteristics of the NPs themselves. Many attempts have been made to form testable hypotheses to describe and predict these structure–activity paradigms, as they can be relevant tools to manage the risk of their introduction into the market.[1] Among the most promising there are 1) the dissolution of metal ions from the NP core, which can subse-

quently interact with toxicity targets, and 2) the potential for electron transfer between the metal atoms on the NP surface and cellular targets, a toxicological mechanism reported as bandgap.[2,3] Whilst these paradigms have found use in predictive risk assessment in *in vitro* testing systems, their application to "real world" environmental conditions requires additional knowledge of the ways in which the receiving environment transforms the NPs. In fact, the toxicological threat posed by NPs to organisms highly depends on both the intrinsic proprieties of nanomaterials and those acquired inside the receiving environment. This greatly limits the extrapolation of toxicological predictions based on structure–activity paradigms established through simple model-systems (*e.g. in vitro* systems) to environmentally relevant scenarios. Thus, the need to consider the environment/nanomaterial-specific transformations makes the assessment of the environmental hazard of NPs a challenging research goal, in spite of the considerable research effort addressing the ecotoxicological impact of nanotechnologies.[4]

College of Life and Environmental Sciences, University of Exeter, EX4 4QD, Exeter, UK. E-mail: s.noventa2@exeter.ac.uk; Tel: +44 (0)1392 263436

1764 | *Environ. Sci.: Nano*, 2018, **5**, 1764–1777

This journal is © The Royal Society of Chemistry 2018

In aquatic environments, the ultimate sinks of many pollutants, the physico-chemical proprieties of NPs can be modified by natural organic matter (NOM), a complex mixture of environmental macromolecules (*i.e.* humic substances (~50%), polysaccharides, lipids, proteins and other organic materials) ubiquitously present in natural waters.[5] Depending on their nature, nanomaterials and organic matter can interact at different strengths and *via* several mechanisms, such as ligand exchange, complexation with acidic and hydroxyl functional groups (*i.e.* carboxyl and phenolic groups), hydrogen bonding, electrostatic interaction, hydrophobic interaction, and cation bridging.[6,7] The formation of a NOM coating on the NPs surface (*i.e.* to form a corona, eco-corona) can alter the toxicological behavior of NPs to aquatic organisms by modifying their surface properties and thus their overall transportation, bioavailability and reactivity.[5,8] In the particular case of the marine environment, the behavior of NPs and the influence of the eco-corona is further impacted by seawater ions.[9] Ions, attracted to the NP surface by opposing charges, can impair both the aqueous stability of NPs and their surface chemical proprieties. The former effect is the consequence of the compaction of the double layer, which decreases the electrostatic repulsion and thus enhances coagulation;[10] the latter is the result of a strong interaction (up to chemical bonding) between the sorbed ions and reactive sites of the NPs' surface.[10]

The aim of this study was to assess the influence of NOM on the *in vivo* toxicological behavior of two metal oxide NPs, ZnO and MnO_2 NPs, under seawater conditions. These nanomaterials are representative of two classes of metal oxide NPs whose toxicological activity has been characterized according to the dissolution paradigm for ZnO and bandgap energy paradigm for MnO_2 NPs.[2,11,12] In our previous study,[12] the effectiveness of these predictive structure-related paradigms was tested under simplified seawater conditions, accounting only for salinity. Using oyster embryo–larvae as a model organism and the induction of oxidative stress as a toxicological pathway, we recorded toxicological activity for ZnO NPs but not for MnO_2 NPs. Among the hypothesized causes of the lack of toxicity of MnO_2 NPs, the adsorption of seawater ions on the reactive sites of MnO_2 NPs was considered with particular attention, after having excluded uptake, cellular internalization or change of the oxidative state of Mn.

Here, we tested whether NOM driven transformation of the model NPs can modulate their *in vivo* toxicity, by influencing their bioavailability and mode of action. To this purpose, we evaluated the ability of NOM to modify the stability of NPs under high salinity conditions. Changes to the aggregation and sedimentation of NPs can alter their interaction with organisms, and thus the extent of ingestion and cellular internalization. Then, we focused on the ability of NOM to interfere with processes at the solid/liquid interface, with possible consequences to the overall efficiency of their mode of action. Thus, we assessed NOM influence on the dissolution of ZnO NPs and release of Zn^{2+} ions, a key factor of ZnO NPs toxicity in aquatic systems. According to the literature, NOM can influence the shedding process *via* ligation of the ZnO NPs' surface; however, there is no consistency about the consequences of this interaction in terms of dissolution rate and overall toxicological outcome. For ZnO NPs in common with other dissolving metal NPs (*e.g.* Ag NPs, CuO NPs, Cu NPs), NOM has been reported to both increase and mitigate the induction of harm, by influencing the dissolution process, the bioavailability of the released toxic ions, or both mechanisms.[13–20]

In the case of MnO_2 NPs, we primarily focused on the interaction between ions and the NP surface, in terms of ion sorption. We checked the capacity of MnO_2 NPs to adsorb ionic constituents of seawater and then we evaluated the ability of NOM to modify the major sorption pattern. Here, the specific hypothesis tested was that the *in vivo* toxicological potential of MnO_2 NPs can be enhanced by the presence of NOM in the solid/liquid interface, by weakening the sorption of seawater ions, keeping the NP surface's reactive site more available for redox reactions. This hypothesis was further explored by pretreating the NPs with a bovine serum albumin (BSA) solution, a process leading to the formation of a BSA coating layer over metal oxide surfaces,[21] to mimic the ageing processes occurring to NPs passing through protein-rich environments (*e.g.* wastewater treatment plants) before entering the marine waters.[22] Finally, attention was given to the possible dissolution of MnO_2 NPs *via* redox reaction with NOM (*i.e.* reductive dissolution), a transformation extensively documented for natural Mn oxide colloids in aquatic environments,[23–27] that here can further complicate the structure and processes at the interface. The influence of these environmental transformations on the toxicological behavior of the test NPs was evaluated through short-term *in vivo* exposures of oyster embryo–larvae. We assessed the induction of oxidative stress as the primary toxicity pathway, and the onset of developmental malformation as a pathological outcome at the whole organism level.

2 Materials and methods

2.1 Nanoparticles

ZnO NPs (NM-112) were obtained from the OECD sponsorship programme for the global safety assessment of nanomaterials (www.nanotechia-prospect.org). The physico-chemical properties were retrieved from the official report,[28] except for the pH at the isoelectric point (pH_{IEP}) which was determined by our group. The MnO_2 NPs were purchased from Skyspring Nanomaterials Inc (Houston, USA, 4910DX) and fully characterized at the NERC Environmental Nanoscience Facility (FENAC, Birmingham, UK). All primary features are summarized in Table S1 of the ESI,† together with the methods used for the characterization (*i.e.* shape and primary size *via* transmission electron microscopy, TEM; crystal structure *via* X-ray powder diffraction, XRD; surface area *via* Branauer, Emmett and Teller, BET, and pH_{IEP} *via* electrokinetic method).

2.2 Test materials

The Suwannee River aquatic NOM (2R101N) by International Humic Substances Society (IHSS) was used as a model NOM

This journal is © The Royal Society of Chemistry 2018

Environ. Sci.: Nano, 2018, **5**, 1764–1777 | 1765

in this study. This reference NOM sample contains both hydrophobic acids (fulvic acids) and hydrophilic acids (humic acids), as well as other soluble organic solutes commonly present in natural waters. It is composed of 50.70% carbon (w/w) and it contains both carboxyl and phenolic groups (for full characterization refer to the supplier's website). Bovine Serum Albumin (BSA) was purchased from Sigma Aldrich.

2.3 *In vivo* oyster embryos exposure

2.3.1 NP seawater suspension in the presence of NOM and BSA. The different scenarios of NOM concentrations (*i.e.* 0, 0.5, 2 and 5 mg dissolved organic matter (DOC) L^{-1}) were set up by adding a NOM stock solution (1 mg DOC mL^{-1} in deionized water, DIW) to 900 mL of artificial seawater (ASW; tropic Marin®SEA SALT, salinity 30.0 ± 0.2 ppt). After 4 h stabilization and immediately prior to the *in vivo* exposures, solutions were dosed with test NP stock suspensions, freshly prepared in DIW (30 s ultrasonication at 90% amplitude with ultrasonic probe – Cole Parmer 130 W Ultrasonic Processor; standard protocol developed under PROPECT project – Ecotoxicology Test Protocols for Representative Nanomaterials in Support of the OECD Sponsorship Programme; http://www.nanotechia-prospect.org). Finally, the volume was adjusted up to 1 L with ASW.

In the case of the BSA experiment, a volume of BSA stock solution was added to the MnO$_2$ NPs stock solution in DIW (*i.e.* BSA concentration in the coating reactor was 17.3 g BSA L^{-1}). After 1 h equilibration, this suspension was added to the exposure chambers (final BSA concentration in the *in vivo* exposure treatments was 0.5 g BSA L^{-1}; no NOM was added in the BSA experiment).

For all NOM and BSA scenarios, the tested NP concentrations were 1 and 3 μM for ZnO NPs, and 50 and 200 μM for MnO$_2$ NPs. Both the test NP concentrations and the NOM to NP ratios did not correspond to modelled or predicted present and future environmental scenarios.[29,30] They were selected based on preliminary trials (data not shown) and a previous study[12] which showed them to regulate the behavior and toxicological potential of the test NPs under marine conditions. Negative controls were undertaken for each NOM and BSA treatment.

2.3.2 Oyster fertilization and *in vivo* exposure of embryos. Conditioned oysters were purchased from the Guernsey Sea Farm Ltd. hatchery (Guernsey, UK). To perform the *in vitro* fertilization, the ICES protocol no 54[31] was followed. Briefly, embryos were obtained from at least two pairs of parental adults. Male and female gametes were recovered by gently cutting the gonads with a sharp scalpel, and the recovered egg suspension was fertilized by adding a few milliliters of sperm. Once the polar body was visible on 80–90% of the eggs, the fertilized eggs were incubated for 2 h at 24 °C, in dark conditions and without aeration. At the 16–32 cell stage, embryos were transferred at a density of 250 embryos mL^{-1} into the exposure chambers. The *in vivo* exposures were carried out in triplicate and under static conditions (30 ppt salinity, pH = 8.1 ± 0.05; 12:12 h light/dark cycle, no aeration). Embryo–larvae were exposed to ZnO NPs for 24 h, whereas to MnO$_2$ NPs for 48 h. At the end of the exposure, embryos were filtered through a 25 μm mesh sieve and aliquots were purposely stored for the biological analyses (samples for genomics and functional analyses were snap frozen in liquid N$_2$ and stored at −80 °C; samples for embryotoxicity assay were fixed in buffered formaldehyde solution; samples for TEM imaging were fixed in 3% glutaraldehyde/2% paraformaldehyde in 0.1 M Pipes buffer at pH 7.2, for 2 h at room temperature, and then kept at +4 °C until embedding).

2.4 Influence of NOM and BSA on the behaviour of NPs in artificial seawater (ASW)

The influence of NOM on the behavior of the test NPs in ASW medium was evaluated in terms of aggregation, sedimentation, dissolution (for ZnO NPs only), and capacity to adsorb ASW ions (for MnO$_2$ NPs only). Unless specified, the comparison was made between NP dispersions which were NOM-free (*i.e.* 0 mg DOC L^{-1}) *vs.* NOM-containing (*i.e.* 5 mg DOC L^{-1}); the BSA coated NP dispersions were also considered in the tests with MnO$_2$ NPs. The behaviour of NPs in DIW was also analyzed as reference. NP suspensions were prepared as described in section 2.3.1. More details about the methods are reported in the ESI.†

2.4.1 Aggregation. Dynamic Light Scattering analyses (DLS; Zetasizer Nano ZS, Malvern Instruments, UK) were carried out to assess the hydrodynamic diameter (HD) of the test-NPs under the exposure conditions. The size of the NP aggregates was tested for all treatments (*i.e.* without NOM, 0.5, 2, 5 mg DOC L^{-1}, BSA). For both nanomaterials, measurements were taken at the concentrations used in the *in vivo* exposure to MnO$_2$ NPs (*i.e.* 50 and 200 μM), as those used in ZnO NPs experiment (*i.e.* 1 and 3 μM ZnO NPs) provided poor analytical signals.

2.4.2 Sedimentation. The sedimentation kinetics of the test NPs was explored by scanning the optical absorbance (280–900 nm) of the test suspension over 48 h. The UV-VIS spectrophotometric measurements were taken at 30 min interval for the first 5 h, then at time 24 and 48 h. They were performed through a 1 cm path light cuvette and by using 200 μM NP suspensions. The results are reported here as sedimentation curves, plotting the absorbance intensity at 370 nm for ZnO NPs and 400 nm for MnO$_2$ NPs *versus* time.

2.4.3 Dissolution. The dissolution of ZnO NPs was assessed by comparing the concentration of Zn^{2+} ions in the ASW medium before and after a ageing period (24 h 24 °C, static condition, triplicates). The released Zn^{2+} ions were separated *via* centrifugal ultrafiltration by using 30 kDa size-exclusion membranes (*i.e.* Microsep™ Advance with Omega™ membrane, PALL), whose pore size allows for the retention of NPs (according to our own trials comparing the performance of 3 kDa and 30 kDa membranes; data not shown) but for the passage of NOM (according to the literature[32]). 2 mL of the recovered filtrates underwent microwave

1766 | *Environ. Sci.: Nano*, 2018, **5**, 1764–1777

This journal is © The Royal Society of Chemistry 2018

assisted acid digestion (2 mL of sample, 1 mL of HNO_3, 1 mL H_2O_2; Ethos EZ, Milestone Inc, Shelton) and then elemental analysis after five-fold dilution with DIW (inductively coupled plasma-mass spectrometry, ICP-MS; Thermo Scientific X Series 2). The ICP-MS method is detailed in ESI.†

2.4.4 Adsorption. The hypothesis of adsorption of seawater ions by MnO_2 NPs was tested according to a modified version of the method used by Murray, 1975.[33] The suite of target ions included both seawater's fundamental constituents and some trace elements (Ca, K, Mg, Na, S, Mn, Fe, Cr, Co, Ni, Cu, Cd, Pb), for which evidence of sorption by Mn oxide minerals-colloids are reported by the literature.[10,33,34] Briefly, sorption was assessed by comparing the concentrations of the target ions in the ASW medium before and after the dispersion of MnO_2 NPs (250 μM) and their ageing for 48 h (24 °C, static conditions, triplicates). At the end of the ageing period, the removal of NPs was carried out *via* centrifugal ultrafiltration with 30 kDa size-exclusion membranes (*i.e.* Microsep™ Advance with Omega™ membrane, PALL).

The concentrations of the target ions were measured by ICP-MS or Inductively Coupled Plasma Optical Emission Spectrometry (ICP-OES, Thermo Scientific iCAP 7400; both instrumental methods are detailed in ESI†), upon microwave digestion and fivefold dilution with DIW.

Possible changes in the sorption pattern due to the formation of NOM-/BSA-corona were evaluated by repeating the test in the presence of 5 mg DOC L^{-1} and with BSA pretreated MnO_2 NPs. 30 kDa size-exclusion membranes were used to remove the NPs and recovered the non-sorbed ions (the pore size was selected based on own trial comparing the performance of 30 kDa and 100 kDa size-exclusion membranes). This experimental design allowed us also to verify the hypothesis of reductive dissolution of MnO_2 NPs, as the occurrence of this transformation is shown by a significant increase in Mn concentration in the medium at the end of the 48 h ageing period.

2.5 Bioavailability of NPs

Thanks to the transparency of the larval shell, the filtration and ingestion of NPs could be visually assessed by screening the presence of NP clumps in the larval digestive track under optical microscopy (Zeiss Axio Observer Inverted Microscope). When these clumps were not visible, the digestive tract was further inspected *via* transmission electron microscopy coupled with energy dispersive X-ray spectroscopy (TEM-EDS; JEOL JEM-2100 LaB6 200 kV TEM with Oxford INCA EDS) to check the possible presence of NPs as smaller aggregates or single particles. TEM-EDS analysis was further carried out to explore the cellular internalization of NPs.

For TEM-EDS imaging, fixed larvae underwent 1.5 h postfixation (1% osmium tetroxide reduced with 1.5% potassium hexacyanoferrate in DIW) before being dehydrated twice with a graded ethanol series. The treated samples were sequentially embedded in Spurr resin (TAAB, Aldermaston, UK) and in BEEM capsules. Then, 80 nm ultrathin sections were produced and collected on pioloform-coated 100 mesh copper TEM grids.

2.6 Toxicity of NPs

The design of the toxicological screening was based on the hierarchical oxidative stress paradigm (tier 1: cellular antioxidant defence; tier 2: pro-inflammatory responses; tier 3: cytotoxicity[12,35,36]) and included endpoints over three levels of biological complexity (*i.e.* organism health status, cellular functioning and gene expression). The progressive impairment of shell calcification and of the development of embryos into D-shaped shell larvae was assessed as a marker of pathogenesis at the organism level. At the cellular level, superoxide dismutase activity (SOD; tier 1) and lipid peroxidation (tier 3) were measured; at the genomic level, the relative expression of four genes was considered (tier 1: metallothionein 2, MT2; mitochondrial superoxide dismutase, SODmt; tier 2: allograft inflammatory factor-1, AIF-1; tier 3: inhibitors of apoptosis proteins, IAPs).

2.6.1 Embryotoxicity. A total of 100 organisms per sample were scored using inverted microscopy (Zeiss Axio Observer Inverted Microscope) to assess the extent of embryotoxicity. Based on the degree of malformation of the shell structures, larvae were classified into the following classes of embryotoxicity (Fig. 1):

• Regularly developed D-shaped shell larvae: larvae possessing a completely formed D-shaped bivalve shell, which may be irregular to some degree (as defined by ICES protocol no 54[31]).

• Deformed D-shaped shell larvae: larvae possessing complete paired hinged valves. Shell is not D-shaped, because of the short and highly deformed hinge; it appears thinner than the regular one under inverted optical microscopy.

• Embryos with signs of arrested shell calcification: embryos presenting the typical morphology of "undeveloped embryos" but carrying hints of calcified shell structures of variable size.

• Undeveloped embryos: rounded embryos showing arrested development at the late stage (*i.e.* cells cannot be distinguished nor counted). No calcified shell structures are visible.

2.6.2 Cell function. Oyster embryo samples were homogenized under ice-cold conditions before undergoing spectrophotometric analyses of SOD activity and lipid peroxidation. Both colorimetric methods were carried out according to the protocol reported by Dogra *et al.*, 2016 (ref. 37) and based on the use of a 96-well plate reader (Tecan Infinite® 200 PRO series plate reader).

Briefly, SOD activity was determined by measuring its ability to inhibit the generation of formazan dye. Xanthine–xanthine oxidase was used to generate superoxide radicals in the system. A standard curve, plotting the percentages of inhibition of formazan dye generation against SOD concentrations, was determined for quantification purpose. The adsorption reading was performed at 573 nm in kinetic mode.

This journal is © The Royal Society of Chemistry 2018

Environ. Sci.: Nano, 2018, **5**, 1764–1777 | **1767**

PROGESSIVE IMPAIRMENT OF SHELL CALCIFICATION

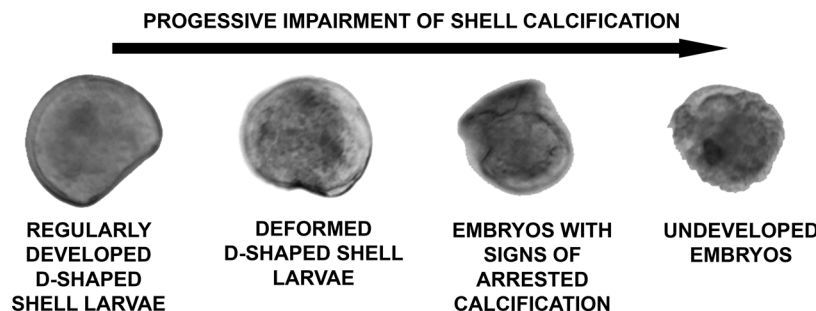| REGULARLY DEVELOPED D-SHAPED SHELL LARVAE | DEFORMED D-SHAPED SHELL LARVAE | EMBRYOS WITH SIGNS OF ARRESTED CALCIFICATION | UNDEVELOPED EMBRYOS |

Fig. 1 Key for the classification of *C. gigas* larvae (24–48 hpf) into the four classes of increasing embryotoxicity.

The oxidative damage of polyunsaturated lipids in cell membranes was assessed through the thiobarbituric acid reacting substances (TBARS) method described by Camejo *et al.*, 1998.[38] The assay quantifies lipid peroxidation in terms of malondialdehyde equivalents (MDA; 530 nm wavelength adsorption) by the use of a standard curve of 1,1,3,3-tetraethoxypropane.

All samples were analysed in triplicate and the results were normalized per mg of cell protein. Total protein concentration was assayed by BioRad's protein micro-assay method, using bovine serum albumin as standard (manufacturer's protocol).

2.6.3 Gene expression (RT-qPCR). Relative expression of the selected genes was determined through reverse-transcription and quantitative polymerase chain reaction (RT-qPCR) analysis. Embryo samples were homogenized through a pestle and total RNA extracted using Trizol, followed by DN-ase treatment (RQ1 RNase-Free DNase, Promega, Southampton, UK; manufacturer's protocol). cDNA was synthesized from 2 μg RNA using oligo dT and M-MLV Reverse Transcriptasis (Promega, Southampton, UK; manufacturer's protocol). The expression of target genes was determined using primer sequences (Table S3 in the ESI†). qPCR analyses were performed in triplicates by using iTaq Universal SYBR Green Supermix (Bio-Rad) and iCycler iQ Real-time detection system (Bio-Rad Laboratories Inc., CA, USA). More details about qPCR conditions and amplification performance are reported in Table S3 (ESI†).

The relative expression of each gene transcript was calculated as described elsewhere.[39] Briefly, the mean C_t value of each biological replicate was corrected for amplification efficiency and compared to the normalisation factor obtained from the expression of two housekeeping genes (*i.e.* elongation factor-1, EF-1; ribosomal protein S18, RS18). For each target gene, the expression ratios between treated samples and control were computed by using the comparative C_t method (*i.e.* $2^{-\Delta\Delta C_t}$).

2.7 Statistical analysis

One-way ANOVA followed by Tukey's test ($p = 0.05$) were used to evaluate NOM/BSA influence in the aggregation state of the two test NPs, in the dissolution of ZnO NPs and in the sorption capacity on MnO_2 NPs. In the adsorption test, the significative sorption of the target ASW's ions on the surface of the MnO_2 NPs was previously evaluated *via* Student's *t*-test ($p = 0.05$).

With respects to the gene expression and cell function data, one-way ANOVA followed by Tukey's test ($p = 0.05$) was initially used to screen the effective stimulation of the target responses by each NP exposure concentrations. Then, for each response which resulted as stimulated by NPs under a specific concentration, the ability of NOM/BSA in modulating the toxicological response was assessed *via* one-way ANOVA followed by Tukey's test ($p = 0.05$). Levene's test ($p = 0.05$) was used to preliminary assess the assumption of homogeneity of variance ($p = 0.05$); non-parametric tests were used whenever the homoscedasticity assumption was missed. The results are reported as mean (±standard deviation) of biological triplicates relative to the associated control.

For embryotoxicity data, the non-parametric ANOVA for rank Chi square test ($p = 0.05$) was used to compare the frequency of the shell deformation classes recorded in the different NOM/BSA scenarios under each NP concentration.

Statistical analyses were performed using STATISTICA 8.0 StatSoft.

3 Results and discussion

3.1 Physico-chemical behavior and transformations of the test NPs in artificial seawater (ASW)

The ZnO NP aggregates formed in the 50 μM dispersions were slightly smaller (≃10%) in the presence of 2 and 5 mg DOC L^{-1} than in its absence (one-way ANOVA followed by Tukey's test, $p < 0.05$; Fig. 2A). No statistical differences ($p > 0.05$) were recorded amongst ZnO NP dispersions with and without NOM at the highest ZnO NPs concentration (*i.e.* 200 μM), where the aggregate size was bigger and the standard deviation was greater. Here, the reduced stabilizing influence of NOM might be due to the lower surface coverage by NOM under conditions of decreasing NOM to ZnO NP ratio.[40–42] Although we were not able to distinguish the aggregation behavior of ZnO NPs under all of the conditions tested (because of poor DLS signals at 1 and 3 μM), the pattern of aggregation suggests that the size of the aggregates could be smaller and NOM could reduce ZnO NP aggregation in the exposure
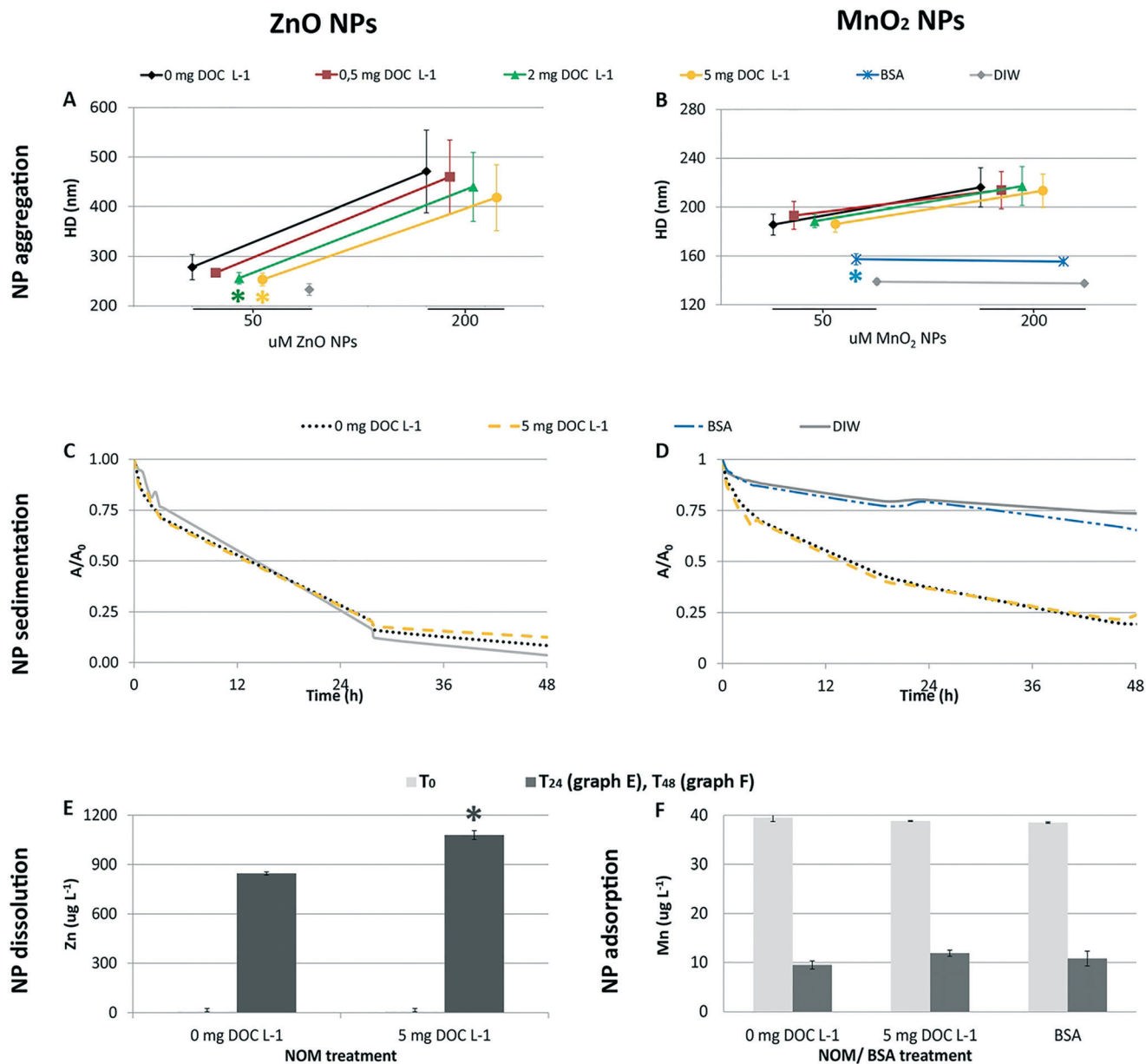
Fig. 2 Influence of NOM and BSA in the behavior of ZnO NPs (left side) and MnO$_2$ NPs (right side) in ASW. Aggregation (A and B): hydrodynamic diameter (HD) of the test NPs in 50 and 200 μM NPs suspensions; (*) marks significant difference (p = 0.05) compared to the corresponding NOM-free NPs dispersion (0 mg DOC L^{-1}); DIW data are plotted to the purpose of comparison, but they were not considered in the statistical analysis. Sedimentation (C and D): sedimentation curves of 200 μM NPs suspensions; the graphs plots the absorbance of the suspensions (at 370 nm for ZnO NPs and 400 nm for MnO$_2$ NPs 48 h) *versus* time; the absorbance at each time point is normalized for the initial absorbance intensity (*i.e.* A/A$_0$). ZnO NP dissolution (E): concentration of Zn^{2+} ions in the ASW medium before (T$_0$) and after (T$_{24}$) the dispersion and ageing of ZnO NPs (250 μM) for 24 h; (*) marks significant difference (p = 0.05) compared to the NOM-free NPs dispersion (0 mg DOC L^{-1}) following the 24 h ageing period. Sorption of Mn^{2+} ions by MnO$_2$ NPs (F): concentration of Mn^{2+} ions in the ASW medium before (T$_0$) and after (T$_{48}$) the dispersion and ageing of MnO$_2$ NPs (250 μM) for 48 h.

chambers, because of the lower ZnO NP concentrations and the higher NOM to ZnO NPs ratio.

With regard to MnO$_2$ NPs, NOM did not influence the aggregation pattern ($p > 0.05$) at the concentrations tested *in vivo* (50 and 200 μM; Fig. 2B). In contrast, BSA treatment affected the aggregation process (one-way ANOVA followed by Tukey's test, $p < 0.05$ for 50 μM; Kruskal-Wallis, $p < 0.05$ for 200 μM; Fig. 2), leading to aggregate sizes similar to that in

DIW. This differential aggregation pattern remained consistent over time, in spite of the progressive enlargement of the aggregates' size (plot reported in the ESI†). The effectiveness of BSA in stabilizing metal/metal oxide NPs has been observed for suspensions in marine water[22] and milder ionic solutions.[43] Its efficiency in providing greater colloidal stability compared to NOM has been reported for MnO$_2$ NPs[44] and other metal oxide NPs[45] under variable ionic conditions (*i.e.*

increasing concentrations of different electrolytes). This is due to the globular architecture of the adsorbed BSA which induces long range steric repulsive forces among NPs.[22,44,45]

The sedimentation profiles recorded for the 200 µM NP suspensions (Fig. 2C and D) highlight that NOM could not counteract the progressive sedimentation of either nanomaterial in the ASW medium. In fact, the sedimentation profiles recorded in the presence and absence of NOM overlapped. In contrast, the BSA coating allowed for an efficient stabilization of MnO_2 NPs (i.e. the sedimentation profile was similar to that recorded in DIW).

The dissolution experiment showed that the presence of NOM promoted the dissolution of ZnO NPs (Fig. 2E). The percentage of Zn shedding its ionic form was $6.5 \pm 0.2\%$ in the presence of 5 mg DOC L^{-1}, and $5.2 \pm 0.1\%$ in its absence ($p < 0.05$). The similar pH values of the two NPs suspensions (pH = 7.95 ± 0.02) ruled out pH as the cause of the enhanced dissolution in the presence of NOM. The ability of organic ligands to promote ZnO NPs dissolution, already observed by Ong et al. (2017),[46] was further studied by Jiang et al. (2015)[47] who found the aromaticity to be the key propriety in the NOM that enhanced dissolution. From a mechanistic point of view, the authors explained the phenomenon as enhanced release from lower size aggregates or ligand promoted dissolution.

A strong adsorption of the ASW Mn^{2+} ions by MnO_2 NPs was evidenced by the significative decrease of Mn concentration in the ASW medium after ageing of MnO_2 NPs for 48 h (i.e. −77% M; Student's t-test, $p < 0.05$; Table 1). Also cobalt ions proved to be removed from the medium via sorption on the NP surface (i.e. −43%; $p < 0.05$), as indicated by the significant reduction of Co concentration in the medium. However, as the initial concentration of Co^{2+} ions in the ASW medium was two orders of magnitude lower than the concentration of Mn ions, the overall amount of Co^{2+} ions sorbed by MnO_2 NPs was lower than the amount of sorbed Mn ions. A quick check of the sorption capacity of ZnO NPs pointed out

that Co^{2+} ions were not sorbed by ZnO NPs (i.e. Co concentrations before and after the ageing of 250 µM ZnO NPs were 0.24 ± 0.02 µg L^{-1} and 0.24 ± 0.01 µg L^{-1}, respectively; $p > 0.05$), whereas Mn^{2+} ions were only slightly adsorbed (i.e. 39.2 ± 0.2 µg Mn L^{-1} vs. 38.0 ± 0.3 µg Mn L^{-1}; $p < 0.05$), suggesting this behavior was specific for MnO_2 NPs. As regards the other target ions, we did not recorded differences in their concentration ($p > 0.05$). In this respect, it is not possible to exclude the possible adsorption of the major cations to some extent, that was not detected as removal from the medium because of their high concentration.

The high capacity of Mn oxide to sorb metal ions (i.e. Mn^{2+}, Zn^{2+}, Pb^{2+}, Co^{2+}, Cu^{2+}, Cd^{2+}, Ni^{2+}, Ca^{2+}, Mg^{2+}, Na^+, K^+) is well documented.[10,34,48–51] The low pH_{ZPC} of MnO_2 NPs (i.e. here 4.8; more details in the ESI†) is considered a key propriety accounting for their high capacity to attract positive charged ions;[49] however, a number of factors, other than electrostatic attraction, control the sorption behavior of Mn oxide (i.e. charge density of metal ions, processes driving the chemical sorption).[10] Our data showing strong selective sorption of Co^{2+} and Mn^{2+} ions are in close agreement with the literature. In the presence of competitive sorbate ions, multivalent cations (i.e. Mn^{2+}, Zn^{2+}, Co^{2+}, Ni^{2+}) are preferentially sorbed over alkaline ions (e.g. Ca^{2+}, Mg^{2+}) with Mn and Co as the most easily sorbed.[10,48,52] The sorption of Mn^{2+} ions has been specifically investigated by Morgan and Stumm (1964).[48] They proved the extraordinary capacity of the oxide for Mn^{2+} sorption (i.e. 0.5 mole of Mn^{2+} per mole of MnO_2 at pH 7.5, and up to 2 moles of Mn^{2+} per mole of MnO_2 at pH 9, in free-salt solutions) and mechanistically explained the phenomenon as surface complex formation or ion exchange.
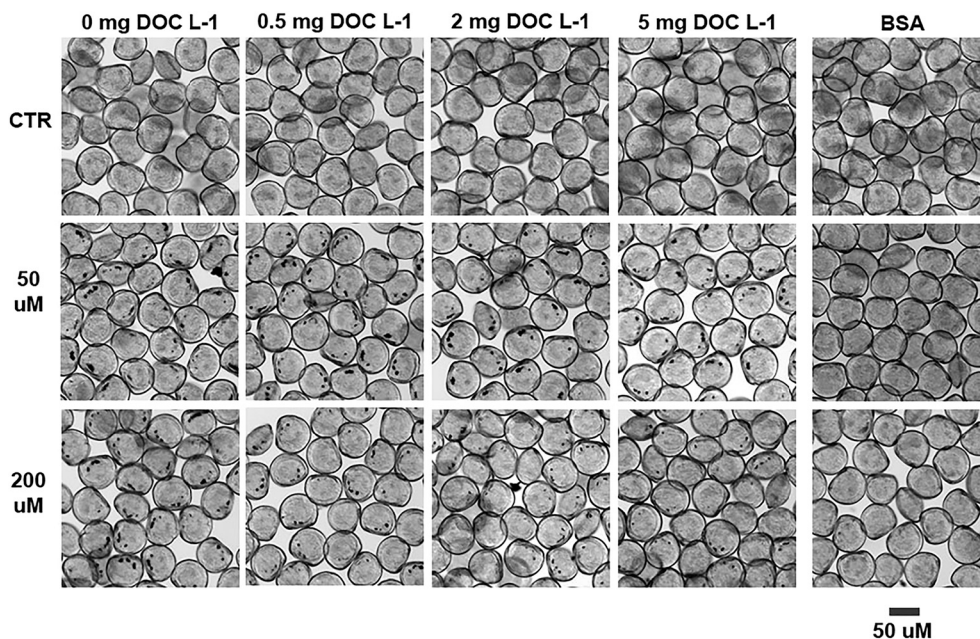
The similar extent of Mn adsorption recorded under the tested scenarios (Fig. 2F; one-way ANOVA, $p > 0.05$) suggests that neither NOM nor BSA could counteract this phenomenon via sorption competition for the ASW Mn^{2+} ions and for the NP surface's reactive sites. This evidence is consistent with the relative position of Mn^{2+} in the stability scale of

Table 1 Sorption test. Concentration of some of the major and minor constituents of the ASW medium before (time 0 h, T_0) and after (time 48 h, T_{48}) the dispersion and ageing of MnO_2 NPs (250 µM) for 48 h. For Ca, K, Mg, Na, and S, the results are reported as signal intensity at the wavelength in the bracket

ASW IONS	Concentration of ASW constituents at T_0 (before the dispersion of MnO_2 NPs)			Concentration of ASW constituents at T_{48} (after the dispersion and ageing of 250 µM MnO_2 NPs for 48 h)			Student's t-test	Percentage of ion removal via adsorption on MnO_2 NP surface
	Mean	St. Dev	RSD	Mean	St. Dev	RSD		
Cr (µg L^{-1})	0.50	0.08	16.6%	0.5	0.1	20.8%	$p > 0.05$	
Mn (µg L^{-1})	36.7	0.6	1.7%	8.5	1.0	11.3%	$p < 0.05$	−77%
Fe (µg L^{-1})	81	3	4.0%	80	5	6.5%	$p > 0.05$	
Co (µg L^{-1})	0.23	0.02	10.1%	0.133	0.006	4.3%	$p < 0.05$	−43%
Ni (µg L^{-1})	6.0	0.2	4.1%	5.9	0.2	2.5%	$p > 0.05$	
Cu (µg L^{-1})	7.9	0.4	4.4%	9	1	11.5%	$p > 0.05$	
Cd (µg L^{-1})	0.05	0.01	26.0%	0.032	0.008	24.1%	$p > 0.05$	
Pb (µg L^{-1})	0.26	0.04	15.2%	0.225	0.01	4.4%	$p > 0.05$	
Ca (315)	538 183	8802	1.6%	526 158	5460	1.0%	$p > 0.05$	
K (769)	112 826	2132	1.9%	109 847	1132	1.0%	$p > 0.05$	
Mg (279)	384 941	2156	0.6%	380 260	2691	0.7%	$p > 0.05$	
Na (330)	66 971	1135	1.7%	65 189	535	0.8%	$p > 0.05$	
S (182.0)	55 116	179	0.3%	54 758	680	1.2%	$p > 0.05$	

Fig. 3 Ingestion of MnO$_2$ NPs by *C. gigas* larvae after 48 h exposure. Optical microscopy images of larvae exposed to MnO$_2$ NP treatments. The black spots visible next to the shell's hinge are clumps of ingested NPs in the digestive tract, indicative of active filtration and ingestion of NPs by oyster larvae. Their identification as MnO$_2$ NPs was attained *via* transmission electron microscopy-energy dispersive X-ray spectroscopy (TEM-EDS) in our previous study.[12]

transitional metal cations forming complexes with organic ligands and Mn oxide. In fact, Mn^{2+} ions form the weakest complexes with organic ligands (the Irving–Williams order;[53]) and the most stable with manganese oxide surfaces.[10] Thus, the strong interaction of Mn^{2+} ions with the oxide surface could have overcome that with the organic components. This is consistent with the distribution of Mn ions in seawater, where only a minor fraction is bound to the organic phase.[54,55]

Finally, it is worth mentioning that the specific strong ion sorption of Mn^{2+} ions did not allow us to evaluate the possible reductive dissolution of MnO$_2$ NPs by NOM (and possibly BSA), a transformation that occurs during the fate of natural manganese oxide colloids in aquatic environments.[25,56]

3.2 NPs bioavailability as described by the evidence of MnO$_2$ NP uptake by oyster larvae

Bioavailability was assessed only for MnO$_2$ NPs as the low concentrations used in the ZnO NPs exposures were not detectable by our imaging analyses.

Except for the organisms exposed to BSA coated MnO$_2$ NPs, the presence of MnO$_2$ NP clumps in larvae' digestive tract (*i.e.* black spots visible through optical microscopy in the proximity of the shell hinge; Fig. 3) proved that larvae effectively filtered and ingested NPs. The similar size and frequency of the spots in the NOM-free and NOM-containing sample suggested that NOM did not substantially modify the ingestion process of larvae (see ESI†).

TEM-EDS analysis was used to verify the possible cellular internalization of MnO$_2$ NPs after ingestion. In agreement with

our previous findings,[12] we identified NPs inside cells, mainly inside single membrane bound vesicles, likely making part of the endo-lysosomal system (an example in Fig. 4, the associated EDS spectrum is reported in the ESI†). Because of the irregular shape and variable electron density of MnO$_2$ NPs, we could neither assess the full extent of the NP uptake nor trace the full biological fate (assessment that would require the execution of the EDS analysis case-by-case, in order to avoid false positives). However, it is worth highlighting that signs of NP cellular internalization were observed both in the MnO$_2$ NP treatments with
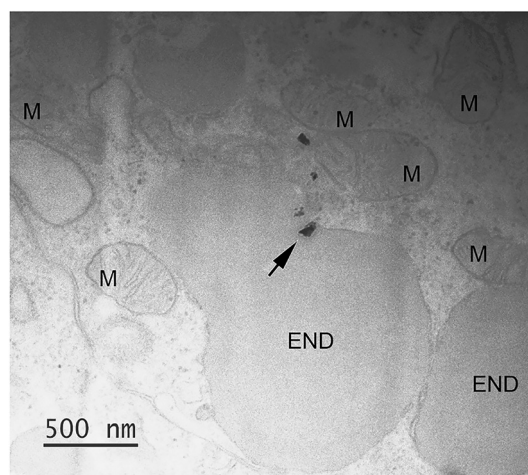
Fig. 4 Cellular internalization of ingested MnO$_2$. Small MnO$_2$ NPs aggregate (arrow), identified *via* EDS analysis, inside a single membrane bound vesicle (END); the associated EDS results are reported in the ESI† (Fig. S7). The picture refers to a larva exposed to 200 μM MnO$_2$ NPs in presence of 5 mg DOC L^{-1}. More abbreviation: M, mitochondrion.

This journal is © The Royal Society of Chemistry 2018

Environ. Sci.: Nano, 2018, **5**, 1764–1777 | **1771**
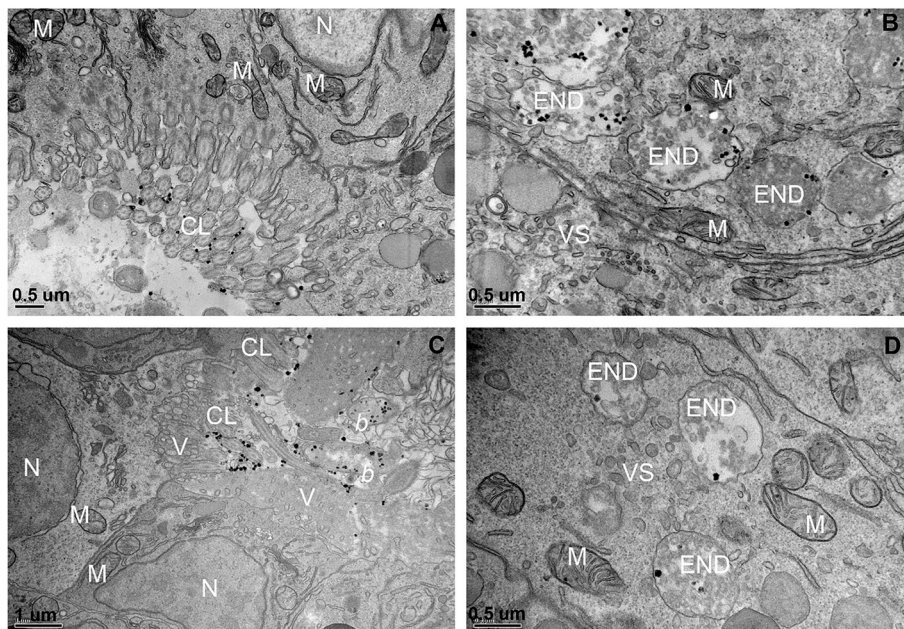
Fig. 5 Representative TEM images showing suspicious electron dense particles excluded to be BSA coated NPs *via* EDS analysis. Suspicious electron dense elements inside the digestive tract and endosomal–lysosomal system of larvae exposed to the BSA-200 μM MnO$_2$ NPs treatment (A and B) and BSA control (C and D). Abbreviations: CL, cilia; N, nucleus; M, mitocondrion; END, endosome-like structure; V, microvilla; VS, cellular vesicles; b, ingested bacteria.
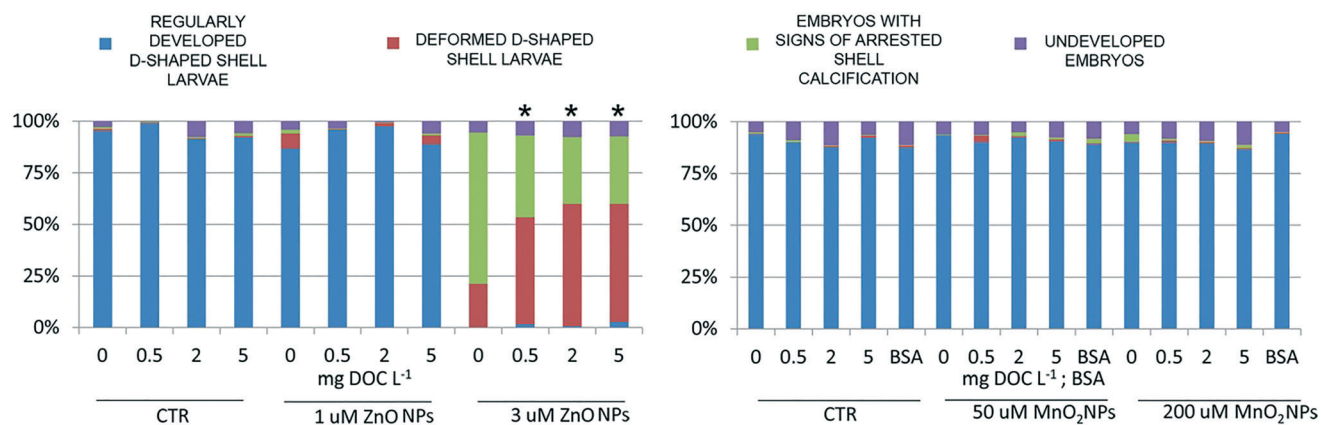
Fig. 6 Results of the embryotoxicity assessment following exposure to ZnO NPs (left side) and MnO$_2$ NPs (right side). Percentage of embryos classified within the four classes of increasing embryotoxicity. (*) Marks samples that significantly differed from the NOM-free NPs dispersion (*i.e.* 0 mg DOC L^{-1}) under each test concentration (Chi square test; $p = 0.05$).
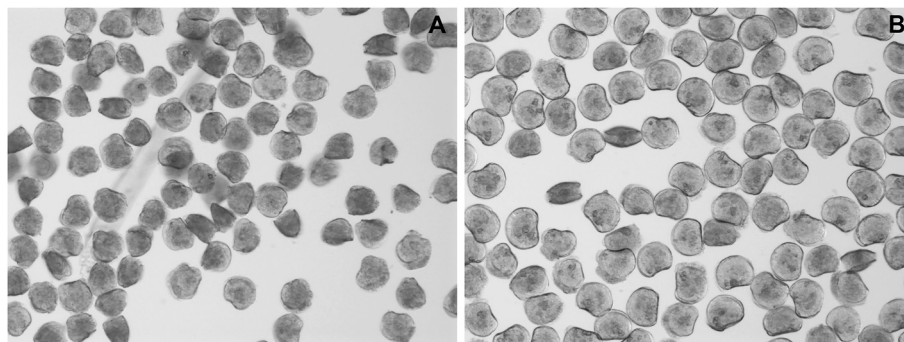
Fig. 7 Representative pictures showing the morphology of larvae exposed for 24 h to 3 μM ZnO NPs in absence of NOM (A) and in presence of 5 mg DOC L^{-1} (B).

and without NOM, without evidencing any particular difference in the internalization pattern and extent.

With regards to the BSA treatments, uptake of NPs was not visible. Larvae did not show clumps of NPs in the digestive tract (Fig. 3); as ascertained *via* TEM, the digestive tracts were clear of NP aggregates and single particles. Some electron dense particles inside the digestive lumen as well as in the endo-lysosomal system, such as those in Fig. 5A and B, were excluded to be BSA coated MnO_2 NPs because they were

found also in the BSA control (Fig. 5C and D) and the EDS analysis did not record a Mn signal (EDS results are reported in the ESI†). This low bioavailability of the BSA treated MnO_2 NPs was unexpected and needs further investigation to be fully explained. Among the possible factors that could have contributed to this phenomenon there are: 1) lower suitability/availability for the filtration and ingestion of the highly dispersed BSA coated NPs by larvae, 2) different rates of filtration and excretion of smaller NP aggregates (*i.e.* lower
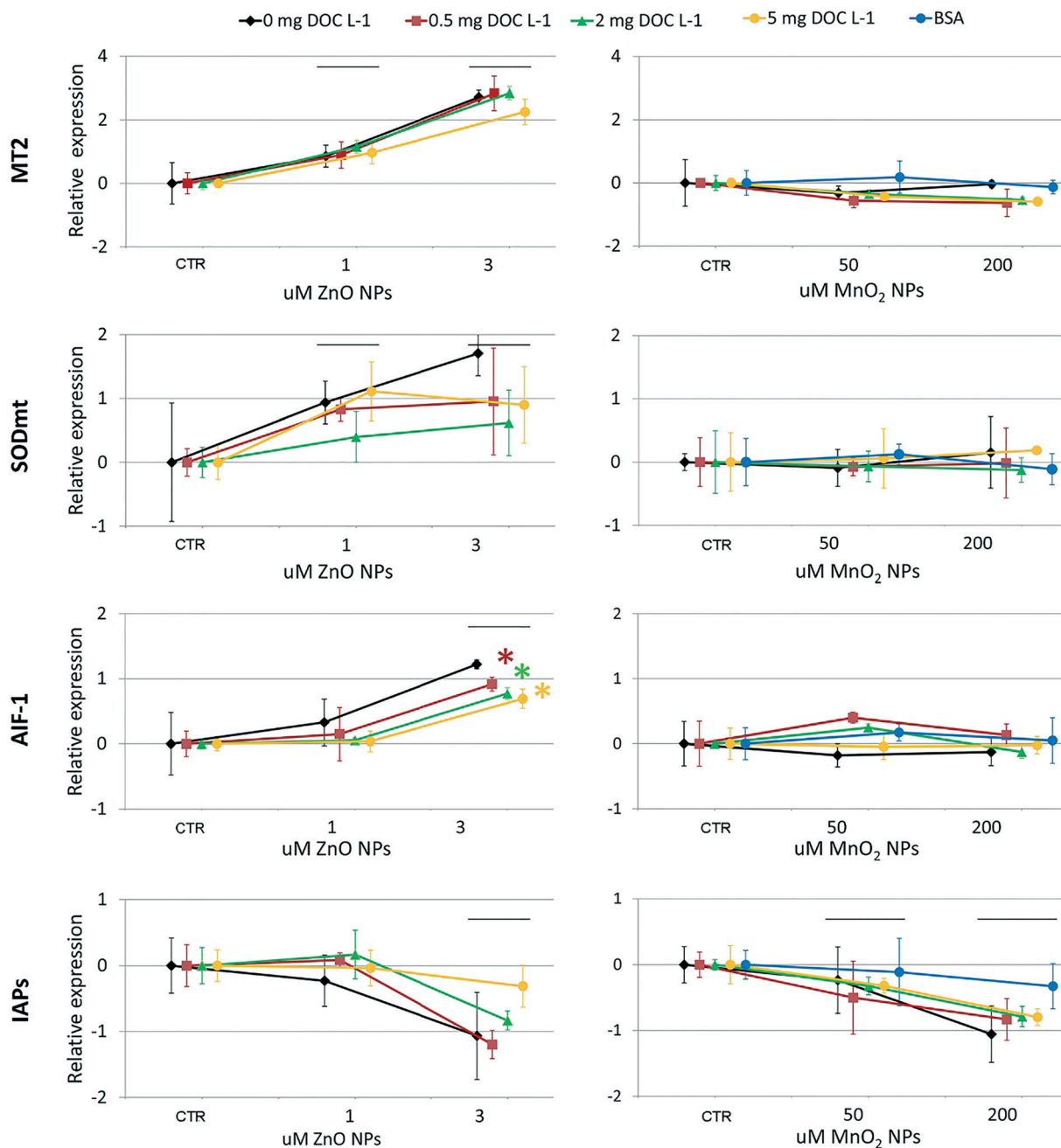
Fig. 8 Results of gene expression analyses following exposure to ZnO NPs (left side) and MnO_2 NPs (right side). Relative expression of target genes as a function of NP concentration ($\log_2$). The straight line (——) marks the NP exposure concentrations which significantly stimulated the target response compared to the control (*i.e.* NP-free dispersions; ANOVA one-way, Tukey HDS post-hoc test, *p*-value = 0.05). (*) marks data that significantly differed from the NOM-free NPs dispersion (*i.e.* 0 mg DOC L^{-1}) under each test concentration (ANOVA one-way, Tukey HDS post-hoc test; *n* = 3, *p*-value = 0.05).

This journal is © The Royal Society of Chemistry 2018

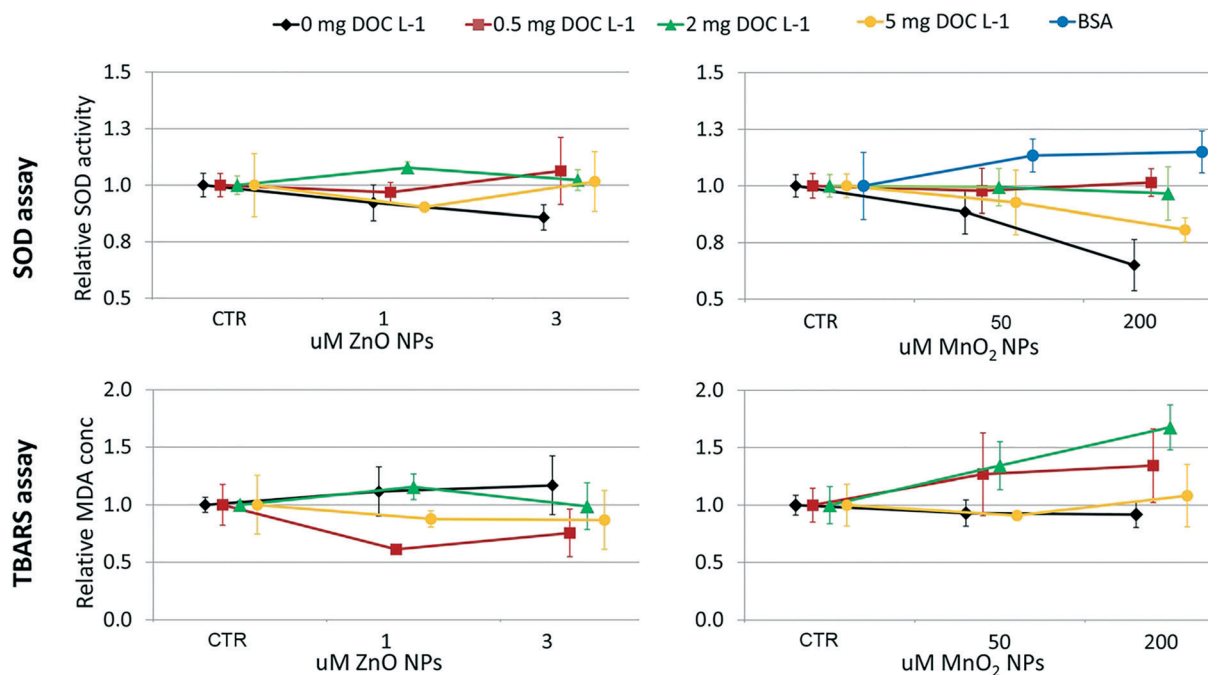*Environ. Sci.: Nano*, 2018, **5**, 1764–1777 | **1773**

Fig. 9 Results of the functional assays following exposure to ZnO NPs (left side) and MnO$_2$ NPs (right side). Relative SOD activity and extent of lipid peroxidation (TBARS assay) as a function of NP concentration. The TBARS results for the BSA-MnO$_2$ NPs treatment was missed for technical faults.

ingestion and/or higher excretion). In spite of their ability to freely swim in the water column, larvae largely settled on the bottom of the exposure chambers (authors' observation) whereas the BSA coated MnO$_2$ NPs remained within the water column because of their slower sedimentation.

3.3 *In vivo* toxicity

The results of the embryotoxicity tests for ZnO NPs (Fig. 6) confirmed the toxicity of this nanomaterial against oyster larvae and showed the ability of NOM to mitigate its toxicity. The presence of NOM reduced the teratogenicity of 3 μM ZnO exposure, a threshold concentration which disrupted shell calcification, but did not completely arrest embryogenesis. In the absence of NOM most of the larvae failed to develop calcified structures (Fig. 7A), whereas in its presence the majority of the organisms developed a complete shell, although thinner and highly deformed (Fig. 7B).

At the genomics level (Fig. 8), exposure to ZnO NPs influenced the expression of all target genes (*i.e.* overexpression of MT2, SODmt, and AIF-1; downregulation of IAPs one-way ANOVA, $p < 0.05$). At the cellular level (Fig. 9), the organisms did not show significant signs of oxidative stress response or cytotoxicity, in contrast to the recorded embryotoxicity, which suggests that, at these concentrations, Zn^{2+} trigger multiple toxicological pathways. Among the possible toxicological pathways involved there might be the impairment of zinc metallo-enzymes, such as alkaline phosphatase (EC 3.1.1.3.1), carbonic anhydrase (EC 4.2.1.1), carboxypeptidase A (EC 3.4.2.1), α-D-mannosidase (EC 3.2.1.2.4), and malate dehydrogenase (EC

1.1.1.37), some of which were found to be involved in the calcification of oyster shells.[57]

In the case of MnO$_2$, toxicological screening showed there to be no significant effects at any level of biological complexity either in the presence or absence of NOM/BSA (Fig. 6–9). The only exception was a modest downregulation of inflammatory mediator IAPs in organisms exposed to 50 and 200 μM, which was not statistically influenced by NOM/BSA (one-way ANOVA, $p > 0.05$).

3.4 Implications of environmental transformations for predictive toxicological paradigms

The toxicological screening of larvae exposed to ZnO NPs confirmed that ZnO NPs can exert toxic effects and that the transformation induced by NOM can mitigate this toxicological potential, which is in accord with previous findings in other species (*e.g.* zebrafish embryos,[46] waterfleas[18]). According to the results of the dissolution test, the presence of NOM did not ameliorate the toxicological behavior of ZnO NPs by reducing dissolution, which, in contrast, was increased. Thus, the mitigation effect could have been associated with the ligation of Zn^{2+} ions by the aromatic carboxylic and phenolic groups of NOM, whose capacity to ligate Zn^{2+} is noted.[5,32,46]

In contrast, the study on MnO$_2$ NPs showed that this nanomaterial has low toxicity on the model organism under ASW conditions. The finding of extensive adsorption of ASW's Mn ions by MnO$_2$ NP strongly support our previous hypothesis that the screening of the NPs' surface by seawater ions could contribute to the lack of toxicological effects in

the MnO_2 NP treated-organisms.[12] In our previous study we observed that the oxidation activity of MnO_2 NPs was quenched in ASW, making the blocking of surface reactive sites by adsorbed counterions a valuable hypothesis to explain the lack of toxicity *in vivo*. Here, we obtained experimental evidence of this strong sorption capacity and we observed that the presence of NOM in the medium did not influenced it, consistently with the similar pattern of *in vivo* uptake and toxicological profile of MnO_2 NPs under different NOM scenarios. Overall this result is in good agreements with studies demonstrating the inhibition effects of adsorbed cations, primarily Mn^{2+}.[52,58,59] In the present study, the remarkable concentration of Mn in the ASW medium, significantly higher than those featuring natural seawater, could have strengthened the adsorption process, heightening the toxicological consequences of this passivation mechanism (*i.e.* the vertical distribution of Mn^{2+} in coastal waters ranges from 1–4 μg Mn L^{-1} in the surface layer, 0.01–2 μg Mn L^{-1} at middle depth, up to 20 μg Mn L^{-1} in the bottom layer;[60–62] the average ocean water concentration is reported as 0.027 μg Mn L^{-1} [53]).

Thus, the case study of MnO_2 NPs supports the suggestion that the sorption capacity of metal oxide NPs can play a crucial role in the overall effectiveness of the bandgap mechanism in seawater. Mn oxides are among the metal oxide minerals with the highest sorption capacity, as expressed by their low pH_{IEP}.[10] Further study could compare the effectiveness of the bandgap mechanism of metal oxide NPs with different sorption capacity in natural seawater, and to ascertain the role of this propriety in the overall efficiency of this structure–activity paradigm to predict toxicity under marine conditions.

4 Conclusion

This study tested the toxicological impacts of two nanomaterials, ZnO and MnO_2 NPs, under seawater conditions. The ability of NOM to change the proprieties and the behavior of NPs in the ASW medium was explored and related to bioavailability and *in vivo* toxicological potential.

We found that NOM played a mitigating role on the toxicity of ZnO NPs by lowering the bioavailability of the released Zn^{2+} ions. As regards MnO_2 NPs, we found that these NPs were not toxic, regardless of the presence of NOM or BSA. The high sorption capacity of MnO_2 NPs for seawater ions was not modified by the presence of NOM or BSA. This supports our previous hypothesis that the sorption capacity of MnO_2 NPs could have a primary role on the overall toxicological inertness of these NPs under seawater conditions, *via* inactivation of surface reactive site and thus the overall bandgap based-mechanism.

Conflicts of interest

There are no conflicts of interest to declare.

References

1 G. Chen, M. Vijver, Y. Xiao and W. Peijnenburg, A Review of Recent Advances towards the Development of (Quantitative) Structure-Activity Relationships for Metallic Nanomaterials, *Materials*, 2017, **10**, 1013.

2 H. Zhang, Z. Ji, T. Xia, H. Meng, C. Low-Kam, R. Liu, S. Pokhrel, S. Lin, X. Wang, Y.-P. Liao, M. Wang, L. Li, R. Rallo, R. Damoiseaux, D. Telesca, L. Mädler, Y. Cohen, J. I. Zink and A. E. Nel, Use Of Metal Oxide Nanoparticle Band Gap To Develop A Predictive Paradigm For Oxidative Stress And Acute Pulmonary Inflammation, *ACS Nano*, 2012, **6**, 4349–4368.

3 C. Kaweeteerawat, A. Ivask, R. Liu, H. Zhang, C. H. Chang, C. Low-Kam, H. Fischer, Z. Ji, S. Pokhrel, Y. Cohen, D. Telesca, J. Zink, L. Mädler, P. A. Holden, A. Nel and H. Godwin, Toxicity Of Metal Oxide Nanoparticles In *Escherichia Coli* Correlates With Conduction Band And Hydration Energies, *Environ. Sci. Technol.*, 2015, **49**, 1105–1112.

4 H. Selck, R. D. Handy, T. F. Fernandes, S. J. Klaine and E. J. Petersen, Nanomaterials in the aquatic environment: An EU-USA perspective on the status of ecotoxicity testing, research priorities and challenges ahead, *Environ. Toxicol. Chem.*, 2016, **35**, 1055–1067.

5 Z. Y. Wang, L. Zhang, J. Zhao and B. S. Xing, Environmental processes and toxicity of metallic nanoparticles in aquatic systems as affected by natural organic matter, *Environ. Sci.: Nano*, 2016, **3**, 240–255.

6 S. Taujale, L. R. Baratta, J. Huang and H. Zhang, Interactions in Ternary Mixtures of MnO_2, Al_2O_3, and Natural Organic Matter (NOM) and the Impact on MnO_2 Oxidative Reactivity, *Environ. Sci. Technol.*, 2016, **50**, 2345–2353.

7 K. Yang, D. Lin and B. Xing, Interactions Of Humic Acid With Nanosized Inorganic Oxides, *Langmuir*, 2009, **25**, 3571–3576.

8 I. Lynch, K. A. Dawson, J. R. Lead and E. Valsami-Jones, Macromolecular coronas and their importance in nanotoxicology and nanoecotoxicology, In *Frontiers of Nanoscience*, ed. J. R. Lead and E. Valsami-Jones, Elsevier, 2014, pp. 127–156.

9 J. Fabrega, S. N. Luoma, C. R. Tyler, T. S. Galloway and J. R. Lead, Silver nanoparticles: Behaviour and effects in the aquatic environment, *Environ. Int.*, 2011, **37**, 517–531.

This journal is © The Royal Society of Chemistry 2018

Environ. Sci.: Nano, 2018, **5**, 1764–1777 | 1775

10 J. W. Murray and P. G. Brewer, Mechanisms of removal of manganese, iron and other trace metals from sea water, In *Elsevier Oceanography Series*, ed. G. P. Glasby, Elsevier, 1977, pp. 291–325.

11 E. Burello and A. P. Worth, A theoretical framework for predicting the oxidative stress potential of oxide nanoparticles, *Nanotoxicology*, 2011, **5**, 228–235.

12 S. Noventa, C. Hacker, D. Rowe, C. Elgy and T. Galloway, Dissolution and bandgap paradigms for predicting the toxicity of metal oxide nanoparticles in the marine environment: an in vivo study with oyster embryos, *Nanotoxicology*, 2018, **12**, 63–78.

13 Z. Wang, J. Li, J. Zhao and B. Xing, Toxicity and Internalization Of CuO Nanoparticles To Prokaryotic Alga *Microcystis Aeruginosa* As Affected By Dissolved Organic Matter, *Environ. Sci. Technol.*, 2011, **45**, 6032–6040.

14 J. Gao, S. Youn, A. Hovsepyan, V. L. Llaneza, Y. Wang, G. Bitton and J.-C. J. Bonzongo, Dispersion And Toxicity Of Selected Manufactured Nanomaterials In Natural River Water Samples: Effects Of Water Chemical Composition, *Environ. Sci. Technol.*, 2009, **43**, 3322–3328.

15 R. Grillo, A. H. Rosa and L. F. Fraceto, Engineered nanoparticles and organic matter: A review of the state-of-the-art, *Chemosphere*, 2015, **119**, 608–619.

16 J. Fabrega, S. R. Fawcett, J. C. Renshaw and J. R. Lead, Silver Nanoparticle Impact On Bacterial Growth: Effect Of pH, Concentration, And Organic Matter, *Environ. Sci. Technol.*, 2009, **43**, 7285–7290.

17 J. Gao, K. Powers, Y. Wang, H. Zhou, S. M. Roberts, B. M. Moudgil, B. Koopman and D. S. Barber, Influence of Suwannee River humic acid on particle properties and toxicity of silver nanoparticles, *Chemosphere*, 2012, **89**, 96–101.

18 P. Mwaanga, E. R. Carraway and P. van den Hurk, The induction of biochemical changes in *Daphnia magna* by CuO and ZnO nanoparticles, *Aquat. Toxicol.*, 2014, **150**, 201–209.

19 D. Cupi, N. B. Hartmann and A. Baun, The influence of natural organic matter and aging on suspension stability in guideline toxicity testing of silver, zinc oxide, and titanium dioxide nanoparticles with *Daphnia magna*, *Environ. Toxicol. Chem.*, 2015, **34**, 497–506.

20 Y. Xiao, W. J. G. M. Peijnenburg, G. Chen and M. G. Vijver, Toxicity of copper nanoparticles to *Daphnia magna* under different exposure conditions, *Sci. Total Environ.*, 2016, **563**, 81–88.

21 S. Fukuzaki, H. Urano and K. Nagata, Adsorption of bovine serum albumin onto metal oxide surfaces, *J. Ferment. Bioeng.*, 1996, **81**, 163–167.

22 M. Levak, P. Burić, M. Dutour Sikirić, D. Domazet Jurašin, N. Mikac, N. Bačić, R. Drexel, F. Meier, Ž. Jakšić and D. M. Lyons, Effect Of Protein Corona On Silver Nanoparticle Stabilization And Ion Release Kinetics In Artificial Seawater, *Environ. Sci. Technol.*, 2017, **51**, 1259–1266.

23 A. T. Stone and J. J. Morgan, Reduction and dissolution of manganese(III) and manganese(IV) oxides by organics: 2. Survey of the reactivity of organics, *Environ. Sci. Technol.*, 1984, **18**, 617–624.

24 A. T. Stone and H.-J. Ulrich, Kinetics and reaction stoichiometry in the reductive dissolution of manganese(IV) dioxide and cobalt(III) oxide by hydroquinone, *J. Colloid Interface Sci.*, 1989, **132**, 509–522.

25 S. Allard, L. Gutierrez, C. Fontaine, J.-P. Croué and H. Gallard, Organic matter interactions with natural manganese oxide and synthetic birnessite, *Sci. Total Environ.*, 2017, **583**, 487–495.

26 C. van der Zee, W. van Raaphorst and E. Epping, Absorbed Mn^{2+} and Mn redox cycling in Iberian continental margin sediments (northeast Atlantic Ocean), *J. Mar. Res.*, 2001, **59**, 133–166.

27 W. G. Sunda and D. J. Kieber, Oxidation of humic substances by manganese oxides yields low-molecular-weight organic substrates, *Nature*, 1994, **367**, 62.

28 JRC64075, *NM-Series of Representative Manufactured Nanomaterials - Zinc Oxide NM-110, NM-111, NM-112, NM-113: Characterisation and Test Item Preparation*, 2011, http://publications.jrc.ec.europa.eu/repository/handle/JRC64075.

29 N. C. Mueller and B. Nowack, Exposure Modeling Of Engineered Nanoparticles In The Environment, *Environ. Sci. Technol.*, 2008, **42**, 4447–4453.

30 F. Gottschalk, T. Sonderer, R. W. Scholz and B. Nowack, Modeled Environmental Concentrations Of Engineered Nanomaterials (TiO_2, ZnO, Ag, CNT, Fullerenes) For Different Regions, *Environ. Sci. Technol.*, 2009, **43**, 9216–9222.

31 D. Leverett and J. Thain, *Oyster embryo-larval bioassay (Revised)*, ICES Techniques in Marine Environmental Sciences No 54, 2013, p. 34.

32 A. Rathgeb, T. Causon, R. Krachler and S. Hann, Determination of size-dependent metal distribution in dissolved organic matter by SEC-UV/VIS-ICP-MS with special focus on changes in seawater, *Electrophoresis*, 2016, **37**, 1063–1071.

33 J. W. Murray, The interaction of metal ions at the manganese dioxide-solution interface, *Geochim. Cosmochim. Acta*, 1975, **39**, 505–519.

34 L. S. Balistrieri and J. W. Murray, The surface-chemistry of δMnO₂ in major ion seawater, *Geochim. Cosmochim. Acta*, 1982, **46**, 1041–1052.

35 A. Nel, T. Xia, L. Mädler and N. Li, Toxic Potential Of Materials At The Nanolevel, *Science*, 2006, **311**, 622–627.

36 H. Meng, T. Xia, S. George and A. E. Nel, A Predictive Toxicological Paradigm For The Safety Assessment Of Nanomaterials, *ACS Nano*, 2009, **3**, 1620–1627.

37 Y. Dogra, K. P. Arkill, C. Elgy, B. Stolpe, J. Lead, E. Valsami-Jones, C. R. Tyler and T. S. Galloway, Cerium oxide nanoparticles induce oxidative stress in the sediment-dwelling amphipod *Corophium volutator*, *Nanotoxicology*, 2016, **10**, 480–487.

38 G. Camejo, B. Wallin and M. Enojärvi, Analysis of oxidation and antioxidants using microtiter plates, In *Free Radical and Antioxidant Protocols*, ed. D. Armstrong, Humana Press, Totowa, NJ, 1998, pp. 377–387.

39 S. Vogeler, T. P. Bean, B. P. Lyons and T. S. Galloway, Dynamics of nuclear receptor gene expression during Pacific oyster development, *BMC Dev. Biol.*, 2016, **16**, 33.

1776 | *Environ. Sci.: Nano*, 2018, **5**, 1764–1777

This journal is © The Royal Society of Chemistry 2018

40 F. Mohd Omar, H. Abdul Aziz and S. Stoll, Aggregation and disaggregation of ZnO nanoparticles: Influence of pH and adsorption of Suwannee River humic acid, *Sci. Total Environ.*, 2014, **468–469**, 195–201.

41 R. F. Domingos, Z. Rafiei, C. E. Monteiro, M. A. K. Khan and K. J. Wilkinson, Agglomeration and dissolution of zinc oxide nanoparticles: role of pH, ionic strength and fulvic acid, *Environ. Chem.*, 2013, **10**, 306–312.

42 S.-W. Bian, I. A. Mudunkotuwa, T. Rupasinghe and V. H. Grassian, Aggregation And Dissolution Of 4 nm ZnO Nanoparticles In Aqueous Environments: Influence Of pH, Ionic Strength, Size, And Adsorption Of Humic Acid, *Langmuir*, 2011, **27**, 6059–6068.

43 S. Dominguez-Medina, J. Blankenburg, J. Olson, C. F. Landes and S. Link, Adsorption Of A Protein Monolayer Via Hydrophobic Interactions Prevents Nanoparticle Aggregation Under Harsh Environmental Conditions, *ACS Sustainable Chem. Eng.*, 2013, **1**, 833–842.

44 X. Huangfu, J. Jiang, J. Ma, Y. Liu and J. Yang, Aggregation Kinetics Of Manganese Dioxide Colloids In Aqueous Solution: Influence Of Humic Substances And Biomacromolecules, *Environ. Sci. Technol.*, 2013, **47**, 10285–10292.

45 F.-B. Hu, Y.-F. Lin, R. Chen, L. Ding and W. Jiang, Effects of humic acid and bovine serum albumin on the agglomeration and sedimentation of oxide nanoparticles, *J. Zhejiang Univ., Sci., A*, 2014, **15**, 643–652.

46 K. J. Ong, L. C. Felix, D. Boyle, J. D. Ede, G. B. Ma, J. G. C. Veinot and G. G. Goss, Humic acid ameliorates nanoparticle-induced developmental toxicity in zebrafish, *Environ. Sci.: Nano*, 2017, **4**, 127–137.

47 C. Jiang, G. R. Aiken and H. Hsu-Kim, Effects of Natural Organic Matter Properties On The Dissolution Kinetics Of Zinc Oxide Nanoparticles, *Environ. Sci. Technol.*, 2015, **49**, 11476–11484.

48 J. J. Morgan and W. Stumm, Colloid-chemical properties of manganese dioxide, *J. Colloid Interface Sci.*, 1964, **19**, 347–359.

49 X. H. Feng, L. M. Zhai, W. F. Tan, F. Liu and J. Z. He, Adsorption and redox reactions of heavy metals on synthesized Mn oxide minerals, *Environ. Pollut.*, 2007, **147**, 366–373.

50 X. Li, G. Pan, Y. Qin, T. Hu, Z. Wu and Y. Xie, EXAFS studies on adsorption–desorption reversibility at manganese oxide–water interfaces, *J. Colloid Interface Sci.*, 2004, **271**, 35–40.

51 S. S. Tripathy and S. B. Kanungo, Adsorption of Co^{2+}, Ni^{2+}, Cu^{2+} and Zn^{2+} from 0.5 M NaCl and major ion sea water on a mixture of δ-MnO_2 and amorphous FeOOH, *J. Colloid Interface Sci.*, 2005, **284**, 30–38.

52 C. K. Remucal and M. Ginder-Vogel, A critical review of the reactivity of manganese oxides with organic contaminants, *Environ. Sci.: Processes Impacts*, 2014, **16**, 1247–1266.

53 F. J. Millero, in *Chemical oceanography*, CRC Press, Boca Raton, 4th edn, 2013, ch. 3, pp. 91–128.

54 S. Hirata, Speciation of dissolved metals associated with organic matter in coastal seawaters, *J. Oceanogr. Soc. Jpn.*, 1983, **39**, 211–219.

55 W. G. Sunda, Measurement of manganese, zinc and cadmium complexation in seawater using Chelex ion exchange equilibria, *Mar. Chem.*, 1984, **14**, 365–378.

56 A. T. Stone and J. J. Morgan, Reduction and dissolution of manganese(III) and manganese(IV) oxides by organics. 1. Reaction with hydroquinone, *Environ. Sci. Technol.*, 1984, **18**, 450–456.

57 A. Brereton, H. Lord, I. Thornton and J. S. Webb, Effect of zinc on growth and development of larvae of the Pacific oyster Crassostrea gigas, *Mar. Biol.*, 1973, **19**, 96–101.

58 Z. Wang and D. E. Giammar, Metal contaminant oxidation mediated by manganese redox cycling in subsurface environment, In *Advances in the Environmental Biogeochemistry of Manganese Oxides*, American Chemical Society, 2015, pp. 29–50.

59 R. F. Carbonaro and A. T. Stone, Oxidation of CrIII aminocarboxylate complexes by hydrous manganese oxide: products and time course behaviour, *Environ. Chem.*, 2015, **12**, 33–51.

60 P. A. Yeats, B. Sundby and J. M. Bewers, Manganese recycling in coastal waters, *Mar. Chem.*, 1979, **8**, 43–55.

61 S. A. Sañudo Wilhelmy and A. R. Flegal, Trace element distributions in coastal waters along the US-Mexican boundary: relative contributions of natural processes vs. anthropogenic inputs, *Mar. Chem.*, 1991, **33**, 371–392.

62 G. A. Cutter, Trace Elements In Estuarine And Coastal Waters - U.S. Studies From 1986–1990, *Reviews of Geophysics*, 1991, vol. 29, pp. 639–644.